RCP is a human breast cancer–promoting gene with Ras-activating function

Jinqiu Zhang,[1] Xuejing Liu,[2] Arpita Datta,[2] Kunde Govindarajan,[3] Wai Leong Tam,[1] Jianyong Han,[1] Joshy George,[3] Christopher Wong,[2] Kalpana Ramnarayanan,[2] Tze Yoong Phua,[2] Wan Yee Leong,[2] Yang Sun Chan,[2] Nallasivam Palanisamy,[2] Edison Tak-Bun Liu,[2] Krishna Murthy Karuturi,[3] Bing Lim,[1,4] and Lance David Miller[2]

[1]Stem Cell and Developmental Biology Program, [2]Cancer Biology and Pharmacology Program, and [3]Computational and Mathematical Biology Program, Genome Institute of Singapore, Singapore. [4]Center for Life Sciences, Beth Israel Deaconess Medical Center, Harvard Medical School, Boston, Massachusetts, USA.

Aggressive forms of cancer are often defined by recurrent chromosomal alterations, yet in most cases, the causal or contributing genetic components remain poorly understood. Here, we utilized microarray informatics to identify candidate oncogenes potentially contributing to aggressive breast cancer behavior. We identified the Rab-coupling protein RCP (also known as RAB11FIP1), which is located at a chromosomal region frequently amplified in breast cancer (8p11–12) as a potential candidate. Overexpression of RCP in MCF10A normal human mammary epithelial cells resulted in acquisition of tumorigenic properties such as loss of contact inhibition, growth-factor independence, and anchorage-independent growth. Conversely, knockdown of RCP in human breast cancer cell lines inhibited colony formation, invasion, and migration in vitro and markedly reduced tumor formation and metastasis in mouse xenograft models. Overexpression of RCP enhanced ERK phosphorylation and increased Ras activation in vitro. As these results indicate that RCP is a multifunctional gene frequently amplified in breast cancer that encodes a protein with Ras-activating function, we suggest it has potential importance as a therapeutic target. Furthermore, these studies provide new insight into the emerging role of the Rab family of small G proteins and their interacting partners in carcinogenesis.

Introduction

The malignant growth of cancer is fueled in part by pathological alterations of the genome that reconfigure the transcriptional programming of cells. This transcriptional restructuring gives rise to the activation of oncogenes and oncopathways and the inactivation of genes and pathways of tumor suppression. In recent years, the magnitude and frequency of transcriptional and chromosomal changes that occur in human cancers have been quantified by DNA microarrays on a comprehensive genomic scale. Correlative analyses of these data have revealed robust associations among gene-expression patterns, copy number alterations, and clinical features of disease (1–7) and may provide a discovery-based framework for uncovering genes with important pathophysiologic roles in cancer (8–13).

We considered the possibility that cancer-promoting genes located at sites of recurrent chromosomal amplifications might be deduced with greater resolving capacity through the integrated analysis of genomic position, gene-expression level, and patient outcome, where the latter allows for statistical associations to be drawn between gene expression and clinical measures of tumor aggressiveness. To this end, we developed a data-mining strategy termed *TRIAGE* (triangulating oncogenes through clinicogenomic intersects) to guide the selection of candidate oncogenes from a large integrated collection of microarray expression profiles of primary breast tumors. Using the TRIAGE approach, we identified RCP (also known as RAB11FIP1) (Ensembl ID number ENSG00000156675), a Rab-interacting protein located at the 8p11–12 chromosomal region frequently amplified in breast cancer, as a prime oncogene candidate. In this work, we describe the discovery of this gene and present functional and biochemical evidence that RCP is a novel breast cancer–promoting gene with RAS-activating potential.

Results

Deducing putative oncogenes through integrative bioinformatics. To identify candidate oncogenes, the TRIAGE methodology combines microarray and clinical outcome data to infer "gene-expression footprints" of recurrent genomic amplicons, relate gene-expression patterns to risk of metastatic recurrence, and evaluate the candidacy of genes based on survival correlations and comparative mRNA dynamics (Supplemental Figure 1; supplemental material available online with this article; doi:10.1172/JCI37622DS1).

In brief, in the first step, microarray expression profiles consisting of 737 primary invasive breast tumors (Table 1) were analyzed by local singular value decomposition (LSVD) to infer the presence and locations of recurrent genomic amplicons (see Methods and Supplemental Methods). This approach is based on the premise that recurrent amplicons can be detected by the

Authorship note: Jinqiu Zhang and Xuejing Liu contributed equally to this work.

Conflict of interest: The authors have declared that no conflict of interest exists.

Nonstandard abbreviations used: AEF, amplicon expression footprint; array-CGH, microarray comparative genomic hybridization; DCIS, ductal carcinoma in situ; DMFS, distant metastasis-free survival; ER, estrogen receptor; *ERBB2*, V-erb-b2 erythroblastic leukemia viral oncogene homolog 2, neuro/glioblastoma-derived oncogene homolog (avian); FWER, family-wise error rate; *LSM1*, LSM1 homolog, U6 small nuclear RNA associated (*Saccharomyces cerevisiae*); LSVD, local singular value decomposition; PEP, principal eigenpeak; RCP, Rab-coupling protein; RNAi Ctrl, control cells stably expressing a random shRNA sequence; RNAi RCP, cells stably expressing shRNA against RCP; TRIAGE, triangulating oncogenes through clinicogenomic intersects.

Citation for this article: *J. Clin. Invest.* **119**:2171–2183 (2009). doi:10.1172/JCI37622.

Table 1
Clinical characteristics of the breast cancer cohorts used to construct the integrated microarray dataset

Characteristic	Uppsala *n* = 251	Stockholm *n* = 159	Oxford *n* = 227	Singapore *n* = 100
Age (years)				
Median	64	56	61	51
Range	28–93	31–87	24–86	29–86
Tumor Size				
<2 cm	112 (45%)	64 (40%)	86 (38%)	16 (16%)
2–3 cm	101 (40%)	71 (45%)	93 (41%)	47 (47%)
>3 cm	38 (15%)	22 (14%)	48 (21%)	35 (35%)
Unknown	0 (0%)	2 (1%)	0 (0%)	2 (2%)
Histologic grade				
Grade 1	67 (27%)	28 (18%)	34 (15%)	11 (11%)
Grade 2	127 (51%)	58 (36%)	91 (40%)	40 (40%)
Grade 3	55 (22%)	61 (38%)	60 (26%)	47 (47%)
Unknown	2 (0.8%)	12 (8%)	42 (19%)	2 (2%)
Lymph node status				
Positive	82 (33%)	60 (38%)	38 (17%)	45 (45%)
Negative	160 (64%)	94 (59%)	183 (81%)	53 (53%)
Unknown	9 (4%)	5 (3%)	6 (3%)	2 (2%)
ER status				
Positive	213 (85%)	130 (82%)	171 (75%)	61 (61%)
Negative	34 (14%)	29 (18%)	48 (21%)	36 (36%)
Unknown	4 (2%)	0 (0%)	8 (4%)	3 (3%)
Metastasis within 5 years				
Yes	42 (17%)	26 (16%)	43 (19%)	15 (15%)
No	183 (73%)	121 (76%)	135 (59%)	35 (35%)
Censored	26 (10%)	12 (8%)	49 (22%)	50 (50%)
Treatment				
No systemic therapy	143 (57%)	33 (21%)	77 (34%)	10 (10%)
Endocrine	80 (32%)	96 (60%)	109 (48%)	23 (23%)
Chemotherapy	24 (10%)	12 (8%)	41 (18%)	30 (30%)
Endocrine and chemotherapy	4 (2%)	18 (11%)	0 (0%)	15 (15%)

coordinate overexpression of involved genes (11, 14) and is supported by evidence that the majority of highly amplified genes in breast cancer are concurrently overexpressed (15). LSVD facilitates the discovery of putative amplicon expression footprints (AEFs) by identifying genomic loci enriched for gene overexpression and, simultaneously, the fraction of tumors where locus-specific overexpression occurs. The output is viewed as principal eigenpeaks (PEPs) that, in effect, mark the location of AEFs and define the tumors that contain them. The peak height (or score) of PEPs depends on the degree of locus-specific overexpression and the number of involved tumors. The highest-scoring PEPs in our analysis mapped predominantly to loci corresponding with known regions of recurrent copy number gain in breast cancer (Supplemental Figure 2), including 17q12, 17q21–24, 11q13, 8p11–12, and Xq28. Though not all peaks identified by LSVD would necessarily be expected to represent true recurrent amplification events, those with highest magnitude and precise genomic overlap with *known* recurrent amplicons were further investigated by the TRIAGE method.

Given that the expression of some oncogenes is known to correlate with poor patient outcomes, genes located within AEFs were assessed for statistically significant associations with distant metastasis-free survival (DMFS) of patients (i.e., the unselected survival analysis in TRIAGE shown in Supplemental Figure 1). However, since it is possible that "passenger genes" located on an amplicon might also correlate with distant recurrence without functionally contributing to tumor aggression and because potent oncogenes may not necessarily require amplification for their activity (11), we reexamined the correlations between gene expression and distant metastasis with the amplicon-containing tumors censored from the analysis (i.e., the TRIAGE selected survival analysis; Supplemental Figure 1). Thus, the combination of unselected and selected survival analyses allows those genes most robustly associated with poor outcome to emerge.

Finally, candidate oncogenes were further discerned through comparisons of mRNA expression patterns. Following the logic that "driving" oncogenes should be relatively highly and consistently expressed in amplicon-containing tumors, the expression levels of genes within AEFs were averaged across the involved tumors and this average was subsequently used to rank genes (where a rank of 1 denotes the highest average expression level). In this way, the expression ranking serves as an additional relative gauge of oncogenic potential at a given locus.

TRIAGE performance was assessed on the AEF with PEP of greatest magnitude identified by our whole-genome LSVD scan (Figure 1A). This PEP delineated a 1-Mb region at 17q12 encompassing about 30 genes and corresponded precisely to the well-characterized amplicon harboring the *HER2/neu* receptor oncogene V-erb-b2 erythroblastic leukemia viral oncogene homolog 2, neuro/glioblastoma-derived oncogene homolog (avian) (*ERBB2*). Notably, the expression footprint of this amplicon has previously been observed in microarray studies and shown to correlate well with the boundaries of the physical amplicon as discerned by microarray comparative genomic hybridization (array-CGH) (11, 15). In tumors exhibiting this AEF, we found a strong enrichment for HER2 positivity by immunohistochemistry ($P < 1.0 \times 10^{-26}$, χ^2 test; Figure 1A), consistent with the hypothesis that this AEF corresponds with the physical 17q12 amplicon in our tumor series. Two genes in this region were found to be significantly associated with metastatic recurrence in patients by both unselected and selected gene-survival analysis, *TCAP* and *ERBB2*, with *ERBB2* also displaying a high expression ranking (Figure 1A and Table 2). Thus, TRIAGE

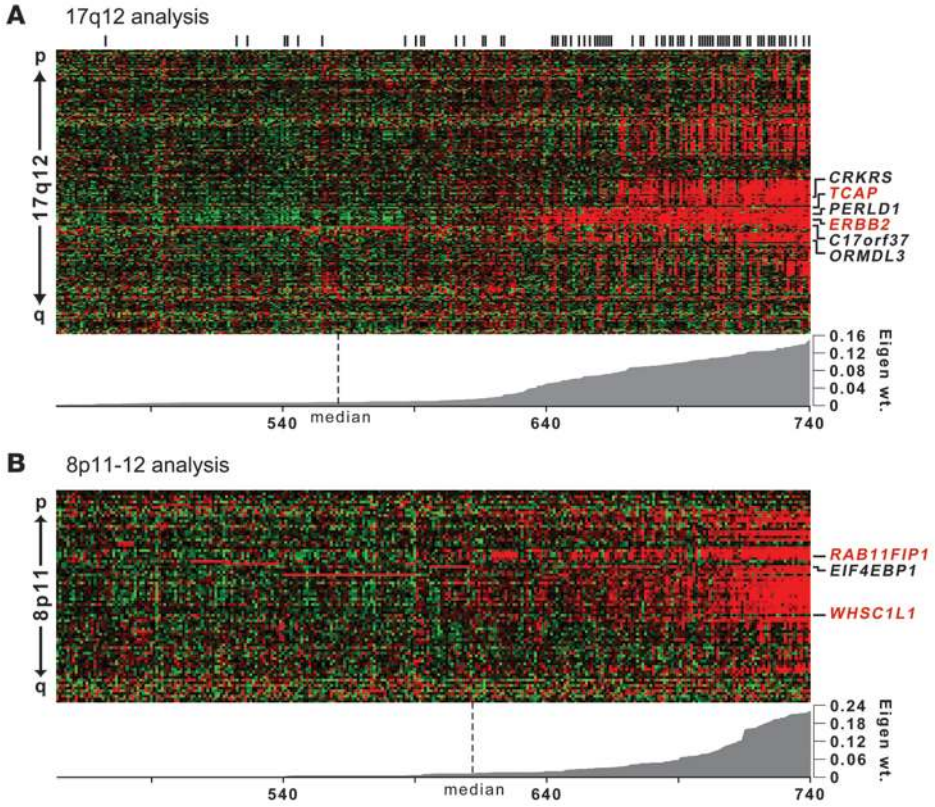

Figure 1
Graphical view of TRIAGE analysis of 17q12 and 8p11–12 amplicons. Expression heat maps of the AEFs at (**A**) 17q12 and (**B**) 8p11–12 are shown. Tumors are arranged in columns, and genes identified by LSVD are organized in rows (in chromosomal order). Red color indicates above-mean gene expression; green denotes below-mean expression. Tumors are ranked by the absolute value of the eigenweight (shown below heat map). Genes with significant survival associations at TRIAGE step 3 are shown to the right. Genes in red indicate top oncogene candidates by TRIAGE (see Table 2). Black vertical bars above the heat map in **A** denote ERBB2 (HER2/neu) positivity by immunohistochemistry.

identified *ERBB2* as a "top candidate" oncogene at the 17q12 locus, independent of its known roles in metastatic breast cancer.

Next, we focused on a second AEF with a high-scoring PEP observed in 17% of the tumors. This PEP mapped to the p-arm of chromosome 8 and delineated a 1.5-Mb region encompassing 22 genes that overlap precisely with the previously described 8p11–12 amplicon known to occur in 10%–25% of breast cancer cases (16–19), the oncogenic drivers of which have not been well characterized. Initially, 3 genes emerged with significant positive associations with metastatic recurrence: *RCP*, *EIF4EBP1*, and *WHSC1L1* (Figure 1B). Two of these, *RCP* and *WHSC1L1*, remained associated following selected survival analysis, with *RCP* having the most significant association with DMFS and highest expression rank (Table 2). RCP expression was also observed to be significantly positively correlated with DMFS ($P = 0.03$) in a second breast tumor cohort (Supplemental Figure 3). Thus, *RCP* was discerned as a plausible oncogene candidate, prompting the investigation of its functional contributions to breast carcinogenesis and tumor progression.

RCP copy number, message, and protein dynamics in cell lines and tumors. RCP was initially identified as an RAB11/RAB4/RAB25–interacting protein, also called RAB11FIP1, with putative physiological roles in endosomal trafficking and receptor sorting (20–22). Though dysregulation of RAB11 (the primary binding partner of RCP) and RAB25 has been implied as a generalized component of several human cancers (23–27), a role for Rab-interacting proteins in cancer has not been described. We therefore examined transcript, protein, and copy number levels of RCP in breast cancer cell lines and primary human tumors. First, by LSVD analysis of microarray expression profiles, 3 cell lines (16%) showed large eigenweights consistent with 8p11–12 amplification, CAMA-1, ZR-75-1, and BT-483 (Supplemental Figure 4A). These 3 lines also showed the highest RCP expression levels as measured by microarray. By Western blot, we observed RCP protein expression in almost all of 14 cell lines screened, with lowest levels in MCF10A noncancerous breast epithelial cells and 3 cancerous cell lines and highest levels in CAMA-1, ZR-75-1, and BT-483 (Supplemental Figure 4B). Finally, genomic analysis by both array-CGH and FISH showed concurrent evidence for amplification of the RCP locus in CAMA-1, ZR-75-1, and BT-483 (Supplemental Figure 4, C and D). Thus, while we observed that amplification of 8p11–12 corresponded with *high-level* overexpression of RCP at both mRNA and protein levels, protein expression of RCP in breast cancer does not appear to be restricted to amplification events, as RCP levels equivalent to those of β-actin and GAPDH were observed in a number of cell lines lacking evidence of genomic amplification.

We next examined RCP protein levels by immunohistochemistry in a panel of breast tumors. As shown in Figure 2A, RCP showed variable expression in invasive ductal carcinomas, ranging from low to highly detectable levels. However, in normal breast epithelium, ductal carcinoma in situ (premalignant), and the weakly aggressive mucinous and medullary histologic types, we consistently observed low to absent RCP staining. Of 60 breast tumor cores, 70% showed detectable RCP staining. To assess whether certain molecular subtypes of breast cancer might show preferential expression of RCP, we compared RCP expression levels across basal-like, luminal A, luminal B, HER2$^+$-like, and normal-like subtypes as previously identified by centroid-based correlations in a cohort of 253 tumors (28). We found that RCP expression was highest in luminal B tumors, lowest in the basal-like subtype, and expressed at intermediate levels in the luminal A, HER2+-like, and normal-like subtypes (data not shown). The differential expression of RCP between basal-like (estrogen receptor–negative

Table 2
TRIAGE results of 17q12 and 8p11–12 candidate genes

Gene symbol	Unselected survival[A]	Selected survival[A]	Expression rank
17q12			
CRKRS	0.006	NS	29
TCAP[B]	0.004	0.038	19
PERLD1	0.039	NS	12
ERBB2[B]	0.010	0.037	3
C17orf37	0.006	NS	2
ORMDL3	0.011	NS	14
8p11–12			
RCP[B]	0.0002	0.004	4
EIF4EBP1	0.006	NS	13
WHSC1L1[B]	0.035	0.049	46

[A]Likelihood ratio test *P* value. [B]Top candidate oncogenes. Unselected survival, selected survival, and expression rank reflect TRIAGE steps 3, 4, and 5, respectively, as described in Supplemental Figure 1.

[ER-negative]) and luminal (ER-positive) tumors ($P < 0.001$, basal vs. luminal A; $P < 0.00001$, basal vs. luminal B) suggests that RCP function may be related in part to some aspect of estrogen signaling. Furthermore, that RCP expression was higher in luminal B (poor outcome) tumors than luminal A (good outcome) tumors ($P = 0.007$) may indicate a specific role for RCP in the more aggressive ER-positive luminal B subtype.

We next examined RCP mRNA levels in another published series of breast tissues for which microarray data was publicly available (29). In this "cancer progression cohort" comprising 6 normal breast specimens, 3 ductal carcinoma in situ (DCIS), 42 primary invasive tumors, and 7 nodal metastases, we observed a highly significant positive correlation with breast cancer progression (Figure 2B). RCP was expressed at lowest levels in normal and DCIS samples, at significantly higher levels in invasive cancer ($P = 0.043$ and $P = 0.035$ for normal vs. invasive and DCIS vs. invasive, respectively; *P* values adjusted for family-wise error rate [FWER]), and at yet significantly higher levels in the metastatic samples ($P = 0.029$ for invasive vs. metastatic; FWER-adjusted *P* value). Notably, similar correlations with disease progression were not observed for the other RAB11FIP family members: -2, -3, -4, and -5. Taken together, these data corroborate the hypothesis that RCP, through mRNA and protein overexpression, may play a functional role in the oncogenic process.

RCP overexpression transforms MCF10A cells. To study the biological effects of RCP expression in noncancerous cells, we used a lentivirus expression system to generate MCF10A cell lines (immortalized mammary epithelial cells) stably overexpressing full-length RCP (MCF10A-RCP) (Genbank accession number NM_025151) or the control vector. While control cells exhibited a flattened morphology and monolayer growth characteristic of normal epithelium, RCP overexpression resulted in dramatic morphological changes, including long pseudopodial projections and a scattered growth pattern occasionally interspersed with foci-like formations reminiscent of transformed fibroblasts (Figure 3A). At confluence, MCF10A-RCP cells exhibited loss of contact inhibition and continuous multilayer growth. Furthermore, immunofluorescent staining revealed that RCP overexpression was associated with loss of E-cadherin at cell-cell junctions, disorganization of F-actin, and gain of fibronectin expression (Figure 3B), suggestive of an RCP-dependent epithelial-to-mesenchymal transition.

To further evaluate the effects of RCP, we exploited the stringent requirement of MCF10A cells for serum and supplemental growth factors to support their proliferation. The stable lines were maintained both in the presence and absence of growth factors. MCF10A-RCP cells were significantly more viable and proliferative in both culture conditions than control cells (Figure 3C and Figure 4A). Intriguingly, in the most stringent medium of 1% FBS without supplemental growth factors (EGF and insulin), the control cells died within 6 days, while MCF10A-RCP cells bypassed cell death and continued to grow (Figure 3C), indicating that RCP can confer growth factor–independent cell growth. Cell-cycle analysis by propidium iodide staining revealed that after 48 hours of serum and growth factor starvation, 93% of control cells were in G_1 phase with only 3% of cells at G_2M. In contrast, 80% of MCF10A-RCP cells were in G_1, with 13% in G_2M, indicating that RCP overexpression can augment cell-cycle progression (Figure 3D).

Next, we examined the capacity of RCP to drive anchorage-independent growth in soft agar colony formation assays. As expected, the control cells failed to produce colonies in soft agar. In marked contrast, however, MCF10A-RCP cells formed numerous colonies after 4 weeks, demonstrating that RCP is able to induce a transformed phenotype (Figure 3E and Figure 4B). Additionally, we observed that RCP overexpression enhanced the migratory potential of MCF10A cells as demonstrated by wound-healing assays (Figure 3F) and transwell assays (Figure 4D).

RCP enhances tumorigenicity in multiple breast cancer cell lines. To study the impact of RCP on tumor cell growth, we modulated its expression in 2 breast cancer cell lines possessing intermediate levels of endogenous RCP. Overexpression of RCP in MCF7 (ER-positive, p53–wild type) cells moderately increased cell proliferation rate, colony-forming activity in soft agar, and invasion through matrigel (Figure 4, A–C). In MDA-MB-231 (MB231; ER negative, p53 negative) cells, RCP overexpression increased colony-forming activity but not the cell proliferation rate, invasion, or migration ability (Figure 4, A–D). Next, we attenuated the endogenous expression of RCP using targeted RNAi constructs. RCP was "knocked down" either by transient transfection with an siRNA construct or by stable transduction of a lentivirus vector expressing an shRNA targeting RCP. RNAi constructs with scrambled sequence were used as controls. Two independent and nonoverlapping siRNAs directed against RCP led to a 40%–80% reduction in protein levels as well as a significant decrease in cell proliferation in MCF7 cells (Figure 4A). Knockdown of RCP in MCF7 cells also significantly reduced colony formation in soft agar (Figure 4B). In MB231 cells, RCP reduction inhibited colony formation but not cell proliferation rate (Figure 4, A and B). In both cell lines, RCP knockdown markedly attenuated invasion and migration (Figure 4, C and D). Together, these results indicate that expression of endogenous RCP in tumor cells can be important for maintaining proliferative, migratory, and/or invasive capacity.

RCP knockdown inhibits tumor formation and metastasis in vivo. We next sought to determine the relevance of RCP expression in tumor formation and progression in vivo using mouse xenograft models. Initially, we constructed models from MCF7, MB231, and MCF10A cells implanted s.c. and bilaterally into hind flanks. While MCF7 cells form moderately malignant tumors in nude mice in the presence of supplemental estrogen, MB231 cells form highly malignant and metastatic tumors in the absence of supplemental hormone.

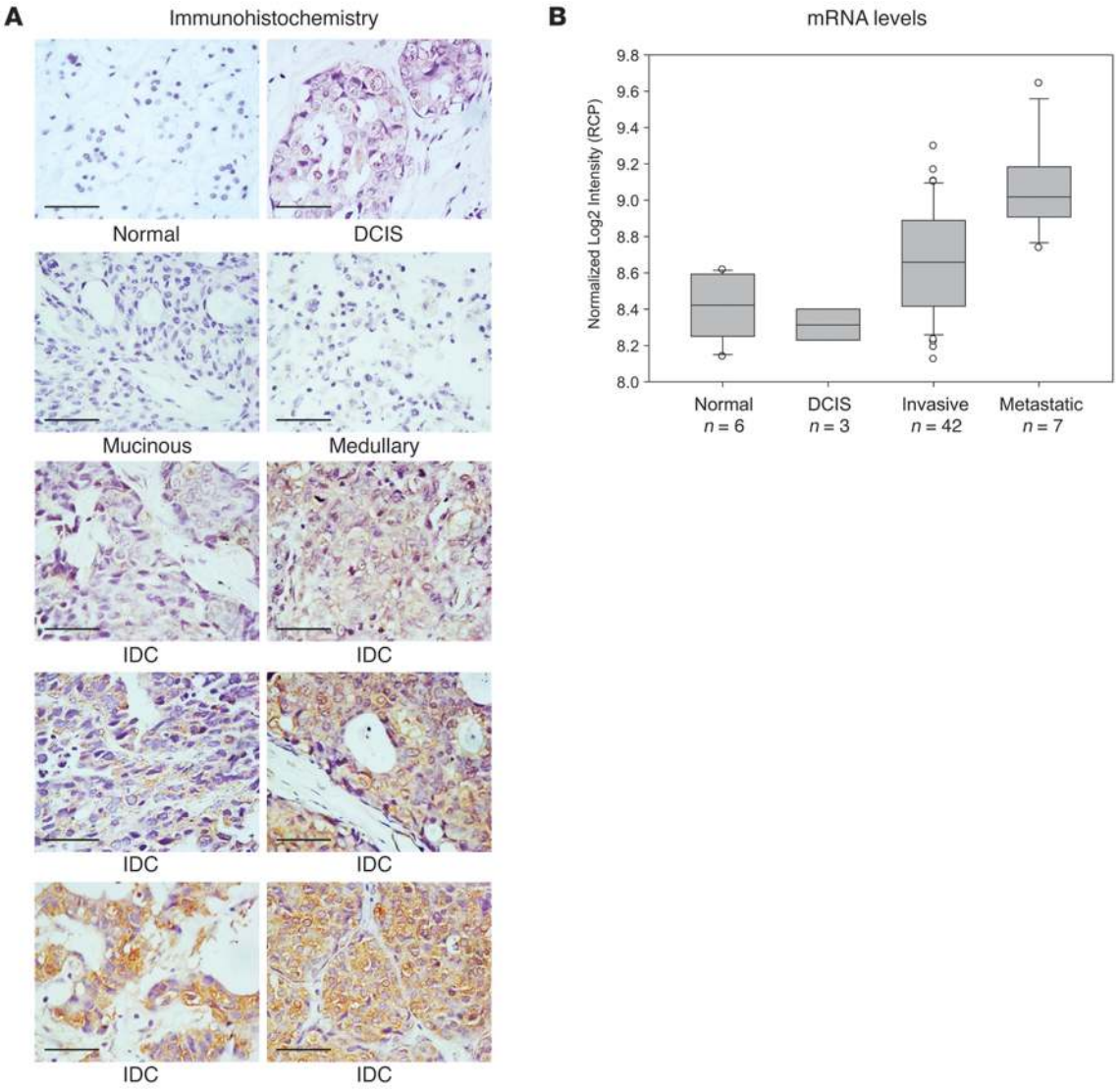

Figure 2

RCP expression correlates with breast cancer progression. (**A**) Immunohistochemical staining of RCP in a panel of breast cancer tissues is shown. Scale bars: 50 μm. IDC, invasive ductal carcinoma. (**B**) Box plots are shown depicting RCP mRNA levels within each breast tissue/cancer type: (a) normal: noncancerous breast tissue from trauma victims (with no malignancy) or mastectomies (adjacent to tumor); (b) DCIS: noninvasive DCIS; (c) invasive: invasive carcinoma of ductal, lobular, medullary, and mixed histologies; and (d) metastatic: tumor metastases dissected from axillary lymph nodes. Boxes: upper and lower boundaries mark the 25th and 75th percentiles, respectively; internal line marks the median. Whiskers (error bars) mark the 10th (lower) and 90th (upper) percentiles, while all values outside of whiskers are shown as circles.

MCF10A is a noncancerous breast epithelial line that lacks innate tumor-forming ability. At 5 weeks after implantation, we observed that MCF7 and MB231 control and RCP-overexpressing cells all formed overt tumors in nude mice, with the latter showing no growth, invasion, or metastatic advantage over the controls (data not shown). Furthermore, neither MCF10A-RCP nor the MCF10A control cells formed tumors (by 7 weeks), suggesting that RCP alone is incapable of initiating tumorigenesis in noncancerous cells.

To investigate the tumorigenic effects of RCP attenuation, we examined the tumor-forming abilities of MCF7 and MB231 cells stably expressing shRNA against RCP (RNAi RCP) or a control sequence (RNAi Ctrl). While all estrogen-supplemented mice implanted with MCF7–RNAi Ctrl or MCF7–RNAi RCP developed overt tumors by 5 weeks, the RNAi RCP cells developed significantly smaller-sized tumors (P = 0.00007; Student's t test) (Figure 5A). Similarly, all mice implanted with MB231–RNAi Ctrl cells developed large tumors; however, only 2 of 8 mice injected with MB231–RNAi RCP cells developed tumors by 7 weeks (i.e., 2 tumors in one mouse and 1 tumor in another) (Supplemental Figure 5A). Notably, these tumors were much smaller than those of the control mice, the average weight being only 1% of the weight of the controls. The knockdown of RCP in tumors was verified by immunohistochemistry (Supplemental Figure 5B).

To further study the tumorigenic properties of RCP in a more orthotopic model, we implanted MB231–RNAi RCP cells or control cells into the fourth inguinal mammary fat pads of each of 9 NOD-

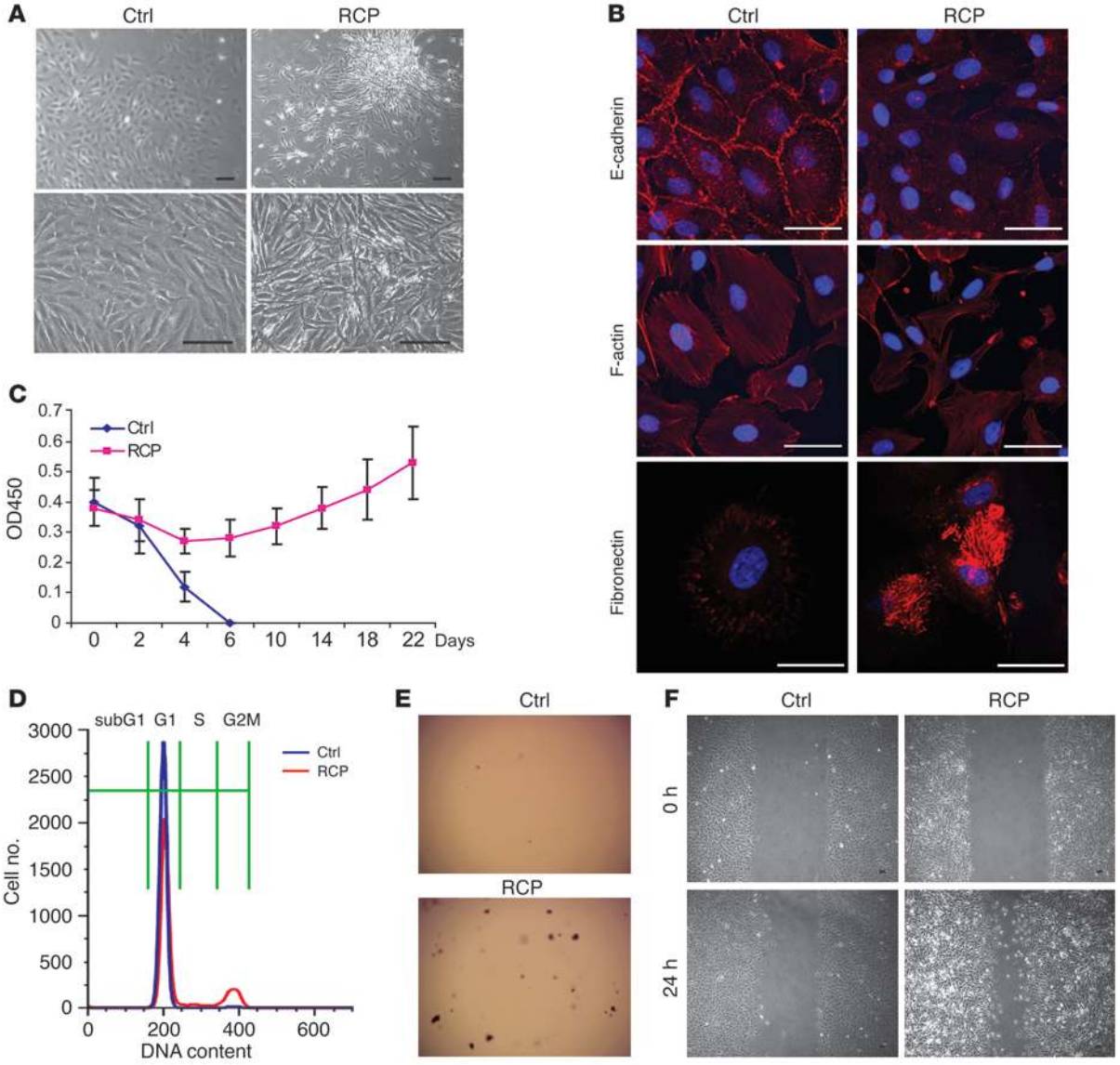

Figure 3

RCP induces oncogenic phenotypes in MCF10A cells. MCF10A control (Ctrl) and RCP overexpressing (RCP) cell lines were assessed for the following biological parameters. (**A**) Cellular growth pattern and morphology. Scale bars: 100 μm. (**B**) Localization of E-cadherin at cell-cell junctions (top panels), organization of F-actin (middle panels), and expression of fibronectin under serum starvation conditions (bottom panels) by immunofluorescence. Scale bars: 50 μm. (**C**) Growth factor–independent proliferation assessed by WST (tetrazolium salt reduction) assay. Data shown represent mean ± SD. (**D**) Cell-cycle progression under serum starvation assessed by flow cytometry. (**E**) Anchorage-independent colony formation in soft agar (example). Original magnification, ×5. (**F**) Cell migration by wound healing (scratch) assay. Scale bars: 100 μm.

SCID mice. Control mice displayed visible tumors at 3 to 4 weeks after implantation and became moribund by 11 weeks due to primary tumor burden, at which point the experiment was terminated. In contrast, the RCP-attenuated tumors were visible only by 6 weeks and were significantly smaller than those in controls by 11 weeks (Figure 5B), recapitulating to a similar degree the reduced-growth phenotype observed in the nude mouse s.c. experiments. Upon in situ examination of the tumors, we observed that both controls and RNAi RCP tumors displayed some degree of stromal and vascular invasion of the mammary pad (Supplemental Figure 5C). However, in the control animals, immunohistochemical staining revealed massive clusters of metastatic epithelial cells in the lungs positive for cytokeratins and hyperchromatic nuclei (Figure 5C). On average, we observed 5 micrometastases per 5-mm section (ranging from 2 to 11 per section for each of 9 animals; Figure 5B). In stark contrast, none of the RNAi RCP mice developed an observable metastasis within the 11-week period. To determine whether this observation was related to the smaller size of the RNAi RCP tumors, we assessed the metastatic potential of control tumors grown to the same average size as the RNAi RCP tumors. In all of 5 animals tested, the size-normalized control tumors (grown for 3 weeks) gave rise to multiple lung metastases, with an average of 2.4 micrometastases per section (Figure 5B), indicating that the reduced metastatic potential associated with RCP knockdown is independent of tumor size. However,

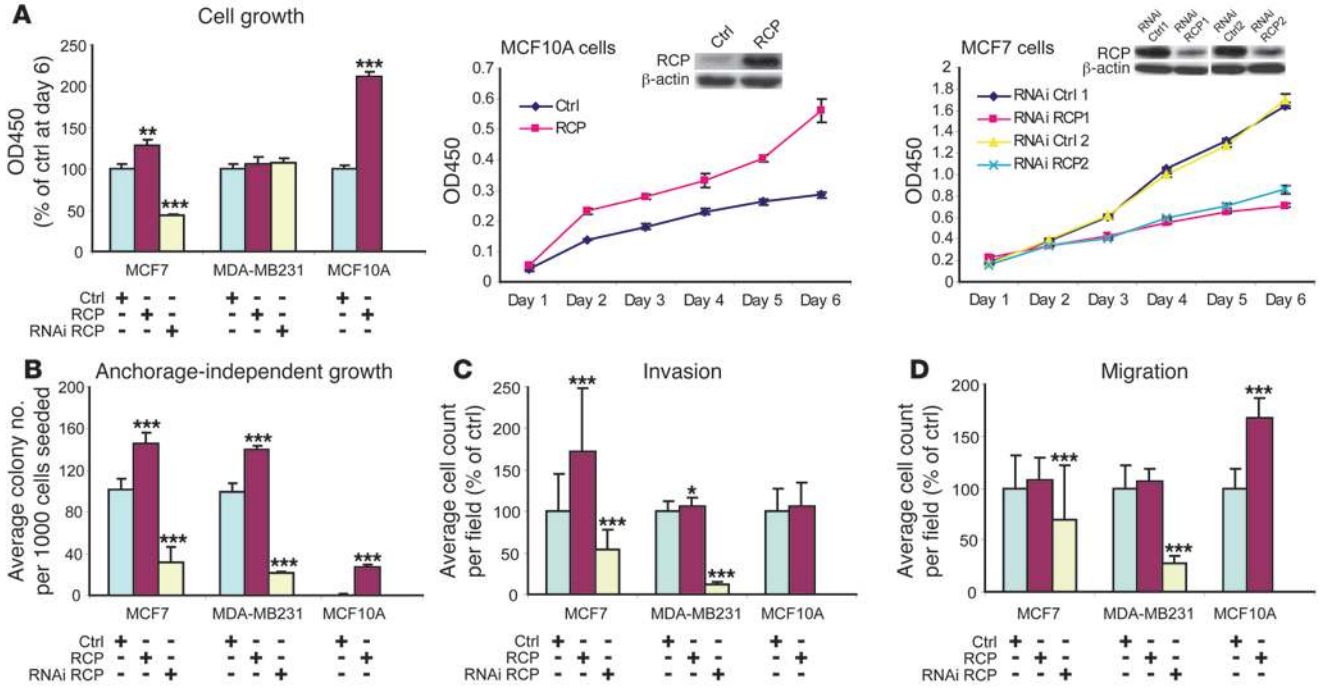

Figure 4

Oncogenic phenotypes of RCP in breast cancer cell lines. (**A**) Effects of RCP overexpression and RNAi-mediated knockdown of RCP on cell proliferation by WST assay. Left panel shows results at 6 days after transfection. Middle panel shows proliferation time course of RCP overexpression in MCF10A cells. Right panel shows proliferation time course of RCP inhibition in MCF7 cells using 2 different RNAi RCP constructs and (scramble sequence) controls. (**B**) Effects of RCP overexpression and inhibition on anchorage-independent colony formation in soft agar. (**C** and **D**) Effects of RCP overexpression and inhibition on (**C**) cell invasion through matrigel and (**D**) cell migration. All error bars computed from mean ± SD. $^{*}P < 0.05$; $^{**}P < 0.01$; $^{***}P < 0.001$, Student's *t* test (2-tailed).

when RNAi RCP tumors were allowed to grow for an extended time period (3.5 months), small lung micrometastases became observable, with an average of 0.4 micrometastases per section (Figure 5B). Whereas multiple large lung metastases were visible by fluorescent imaging in the control mice (via lentiviral GFP signal), none were observed in the RNAi RCP mice (Figure 5C). Thus, the targeted knockdown of endogenous RCP expression not only significantly reduced tumor growth rate (of both estrogen-dependent and -independent human breast tumors) but also markedly attenuated the metastatic spread of breast cancer cells.

RCP stimulates ERK phosphorylation and H-RAS activation. To gain insight into the mechanisms through which RCP exerts its oncogenic effects, we determined whether RCP expression (or knockdown) could activate (or inactivate) signaling through either ERK or AKT, 2 major pathways known to regulate malignant cell growth. RCP-overexpressing MCF10A cells showed enhanced phosphorylation of ERK compared with controls (Figure 6A) but did not appear to enhance AKT phosphorylation (Supplemental Figure 6). Similarly, overexpression of RCP in both MCF7 and MB231 cells enhanced ERK phosphorylation, while knockdown of RCP inhibited ERK phosphorylation (Figure 6A) but not AKT phosphorylation (Supplemental Figure 6).

To determine whether RCP-induced ERK activation was associated with the proliferative advantage of MCF10A-RCP cells, we treated MCF10A cells with U0126, a potent MEK/ERK inhibitor. While control cells displayed low phosphorylation of ERK across a range of U0126 concentrations, ERK phosphorylation status in MCF10A-RCP cells was concentration dependent (Figure 6B). At 30 μM of U0126, RCP-induced phosphorylation of ERK was reduced to baseline (same level as control), while RCP levels remained unaltered. Importantly, the MCF10A-RCP cells attenuated for ERK phosphorylation by 30 μM U0126 showed a reduction of proliferation down to control levels despite high RCP expression (Figure 6B), suggesting that the RCP proliferation phenotype is dependent on activation of the MAPK pathway via phosphorylation of ERK. However, we note that this does not rule out the possibility that the RCP phenotype is also dependent on other pathways that drive proliferation.

As RCP is known to physiologically interact with and regulate RAB11, a RAS-related GTP-binding protein, we investigated the possibility that RCP may mediate ERK phosphorylation through an interaction with the structurally and functionally conserved RAS GTPases. RAS proteins exist in an active, GTP-bound state and an inactive, GDP-bound form. The RAS-binding domain of RAF1 preferentially binds the activated form of RAS and thus provides a basis for measuring RAS activity. In the 3 cell lines studied (MCF10A, MCF7, and MB231 – all expressing wild-type H-RAS), overexpression of RCP resulted in a marked increase in activated, GTP-bound H-RAS (Figure 6A). Conversely, RNAi knockdown of endogenous RCP reduced H-RAS activation to nearly undetectable levels in MB231 and MCF7 cells (Figure 6A). Intriguingly, neither overexpression nor knockdown of RCP altered N-RAS or K-RAS activation levels in these cell lines (Supplemental Figure 7). Furthermore, coimmunoprecipitation experiments revealed evidence for a specific molecular interaction between H-RAS and RCP. In MCF7 cells overexpressing flag-tagged RCP, both exogenous and

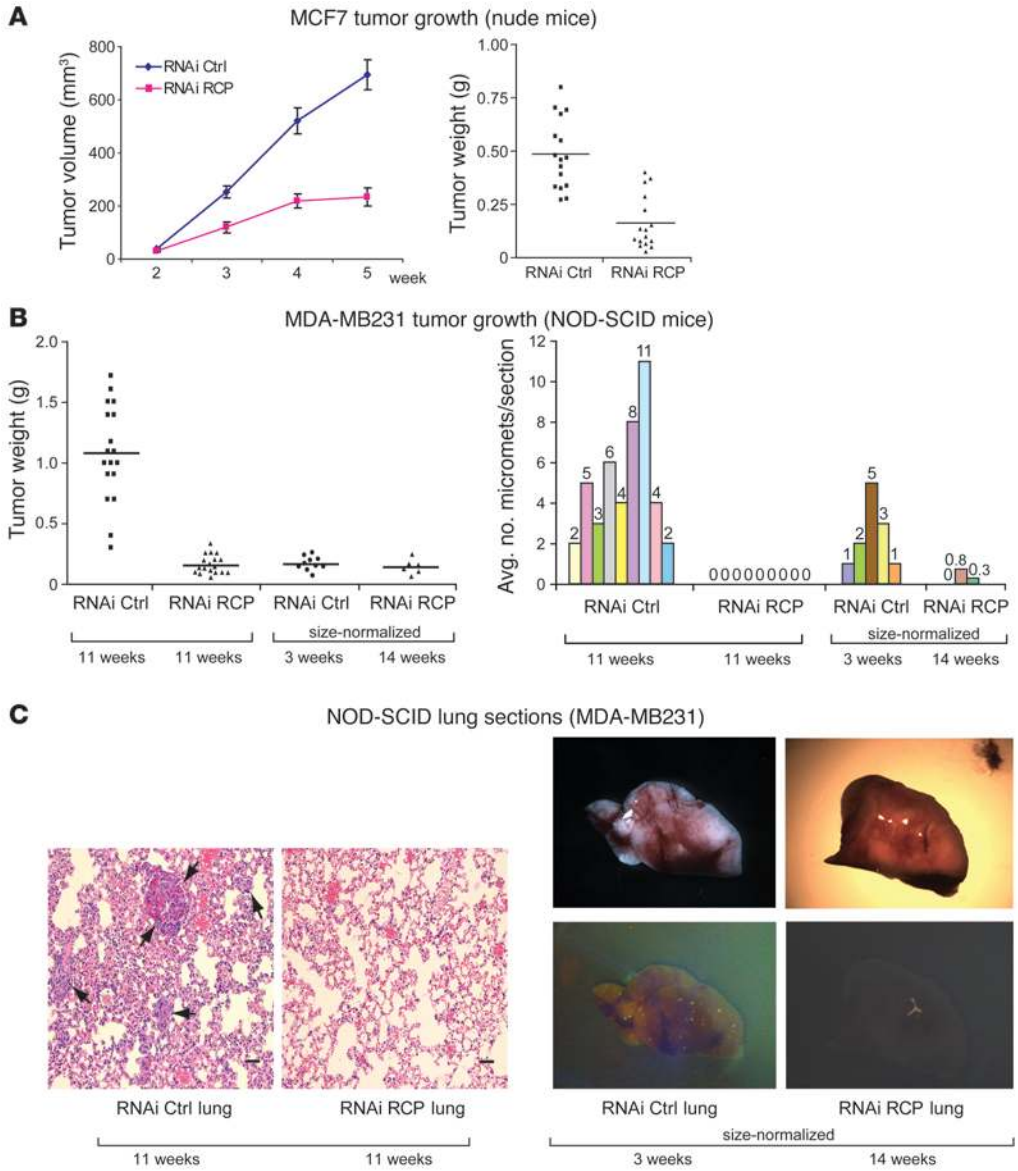

Figure 5
RCP knockdown attenuates tumor formation and metastasis. Effects of RCP inhibition on tumor growth using (**A**) MCF7 cells in nude mice and (**B**) MB231 cells in NOD-SCID mice are shown. (**A**) Left panel shows mean tumor volume plotted as a function of time (mean ± SEM). Right panel shows tumor weight plotted at 5 weeks; mean weight indicated by solid line. (**B**) Left panel, tumor weight plotted at indicated number of weeks; mean weight indicated by solid line. Right panel, the average number of lung micrometastases per section is shown. (**C**) Representative lung sections and fluorescently imaged whole lungs (right panel) of NOD-SCID mice are shown. Micrometastases are indicated by arrows. Scale bars: 200 μm.

endogenous H-RAS could be precipitated together with RCP by anti-FLAG antibody (Supplemental Figure 8A). Additionally, both overexpressed and endogenous H-RAS immunoprecipitated by anti–H-RAS antibody could precipitate endogenous RCP (Supplemental Figure 8B). Together, these data indicate that RCP modulates not only ERK phosphorylation but also H-RAS activation and that the latter may occur via a specific interaction between RCP and H-RAS.

Discussion

Genome-wide microarray analysis of primary tumors has enabled the discovery of novel, clinically relevant tumor subtypes defined by unique patterns of gene expression (1, 2, 6, 30). More recently, however, the inverse of this concept has been explored through bottom-up analytical strategies that seek to identify *gene subtypes* with functional roles in tumorigenesis. These strategies probe the conditional relationships between gene expression and clinical and genomic features of cancer. Adler and colleagues used a genetic linkage approach (stepwise linkage analysis of microarray signatures) to uncover transcriptional mechanisms driving the expression of a prognostic "wound signature" in breast cancer (9). Their work led to the discovery that MYC (at 8q24) and CSN5 (at 8q13) functionally interact to regulate transcription of the wound-response genes. In the present work, we have built on this concept of data integration and functional discovery and identified RCP, located on the 8p11–12 recurrent breast cancer amplicon, as a novel breast-cancer promoting gene with Ras-activating potential.

Amplification of the 8p11–12 locus has been observed in approximately 10%–25% of breast tumor cases (17, 19, 31, 32) and 15% of breast cancer cell lines (17, 18) and has been associated with poor patient survival and short interval to distant metastasis (11, 18, 19, 33). Recently, this amplicon has been the focus of several functional genomics investigations involving primary breast tumors and cell lines (16–18). Using a high-resolution BAC microarray specific for chromosome 8p, Gelsi-Boyer and colleagues (18) determined that the 8p11–12 amplicon actually comprises 4 well-demarcated

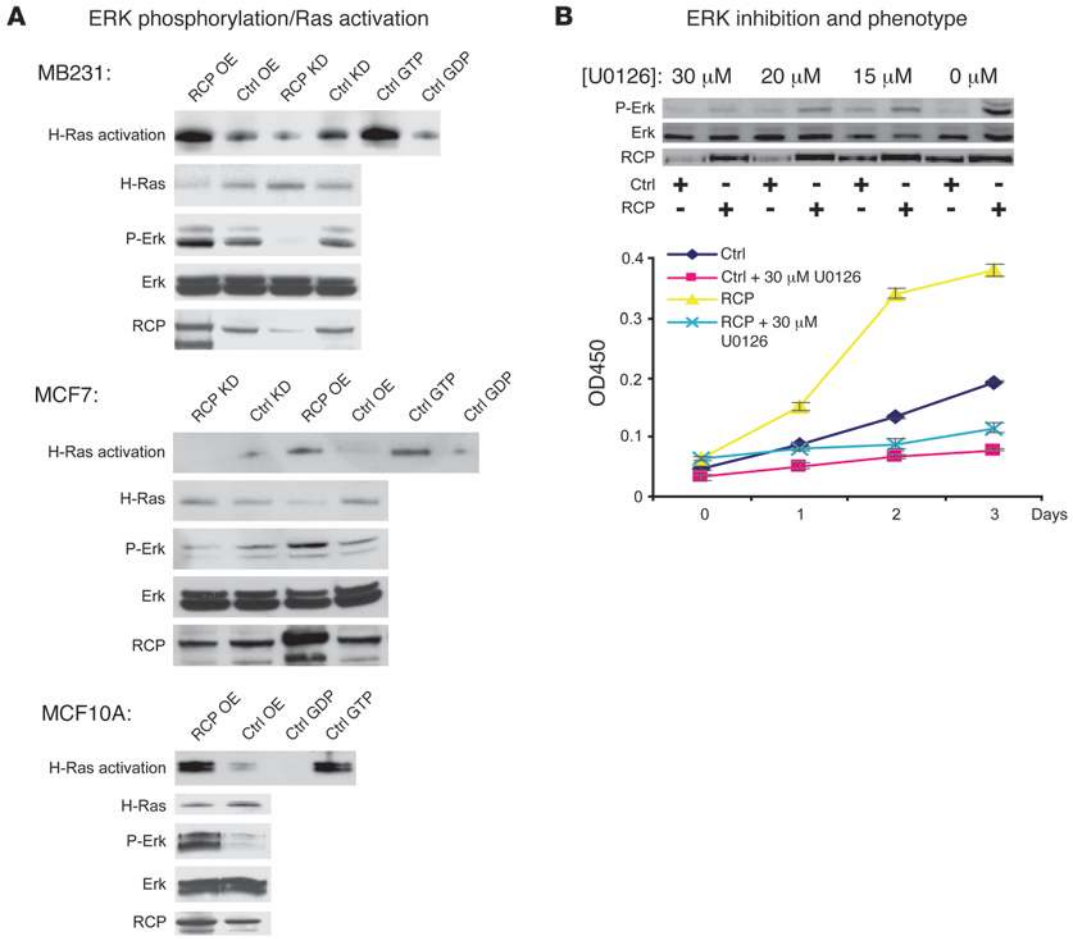

Figure 6

RCP-mediated ERK phosphorylation and H-RAS activation. (**A**) Western blots of H-RAS activation (GTP-bound H-RAS), total H-RAS, ERK phosphorylation status (P-Erk), total ERK, and RCP protein levels in MB231, MCF7, and MCF10A cells are shown in the context of RCP overexpression (RCP OE), RCP knockdown (RCP KD), and controls (CON). (**B**) Inhibition of RCP-mediated ERK phosphorylation in MCF10A cells by the MAPK inhibitor U0126 (upper panel) and U0126-mediated inhibition of the RCP proliferation phenotype (lower panel; mean ± SD).

subamplicons, termed A1, A2, A3, and A4, that share minimal overlap. The authors of this and other studies have proposed a number of candidate oncogenes in this region based on strong correlations between gene amplification and mRNA overexpression (16–18). Cumulatively, these studies have identified *ZNF703 (FLJ14299), ERLIN2 (SPFH2), PROSC, BRF2, RCP,* and LSM1 homolog, U6 small nuclear RNA associated (*Saccharomyces cerevisiae*) (*LSM1*) as having the strongest correlations between amplification and overexpression, with all but *LSM1* localizing to a 1-Mb "minimal amplicon" (17) and overlapping precisely with the A1 subamplicon (18). Notably, the genes identified by LSVD in our study specifically comprise the A1 and A2 subamplicons and thus include the "top candidate" oncogenes described by these earlier studies.

Of the other candidate oncogenes at this locus previously shown to possess some transforming properties in breast epithelial cells (34, 35), *LSM1*, *BAG4*, and *C8orf4 (TC1)* all reside primarily on the A2 and A3 subamplicons (18). *RCP*, in contrast, is located closer to the core of the A1 amplicon on the 1-Mb minimal amplicon (17) and is the first in this region to be functionally characterized as an oncogene.

RCP was originally identified as a binding partner of RAB25, RAB11, and RAB4, members of the Rab family of proteins (20, 21). The Rab proteins belong to the larger family of Ras-related small G proteins (including the Rho-related proteins) that regulate a wide range of basic cell functions including cytoskeletal organization and cell morphology, cytokinesis, vesicle transport and secretion, cell-cycle progression, and cell differentiation (36). Several of these proteins and their regulators and effectors have emerged as potential mediators of carcinogenesis and cancer progression (23–26, 37, 38). Among them, RAB25, which is frequently amplified in breast and ovarian cancers, has been shown to enhance proliferation and apoptotic resistance in vitro and tumor formation in vivo (26). The RAB proteins play a central role in membrane trafficking and organelle compartmentalization, and RAB11, RCP's primary binding partner, is specifically involved in membrane protein recycling (39). RAB11 has been implicated in cell migration, and disruption of RAB11 pathways compromises migration in different cell types (25, 38, 40). Furthermore, the competitive inhibition of RAB11 function has been shown to specifically decrease hypoxia-induced invasiveness of breast cancer cells (25) and to alter trafficking of membrane receptors involved in invasion such as $\alpha_6\beta_4$ integrin, EGFR, CXCR2, and PKC-α (38).

In the present work, we observed correlations between RCP expression, amplification, and tumor aggressiveness in both cell lines and primary tumors. First, examination of RCP mRNA levels in breast tumor expression profiles revealed a strong correlation between RCP overexpression and in silico predictions of chromosomal amplification. Similarly, both RNA and protein levels of RCP were found elevated in breast cancer cell lines with verified 8p11–12 amplification, consistent with previous observations (17–19), and more recently, those from Neve and colleagues (41), who found a highly significant correlation between RCP expression and amplification of its loci ($P = 0.004$ in cell lines; $P < 0.0001$ in primary tumors). By immunohistochemistry, we observed that RCP protein was variably expressed in primary invasive breast cancers (from low- to high-intensity staining) but underexpressed in noncancerous (normal), noninvasive (DCIS), and less aggressive histologic types (mucinous and medullary carcinomas). Consistent with this observation, we also observed statistically significant gains in RCP mRNA expression in transition from normal/DCIS to invasive cancer as well as from invasive cancer to metastatic breast cancer. Taken together with our initial observation that RCP expression is significantly correlated with distant metastasis in patients, these findings suggest a role for RCP in tumor formation and metastatic progression.

Through functional analysis of RCP, we discovered a broad range of cancer-promoting effects linked to RCP expression. In noncancerous mammary epithelial cells, RCP overexpression conferred both growth factor– and anchorage-independent growth as well as increased cell motility and migration, suggestive of a contributing role for RCP in the transformation process. In breast cancer cell lines, attenuation of endogenous RCP by RNA inhibition not only reduced anchorage-independent growth and invasion but significantly diminished tumor formation and metastasis in mice. While overexpression of RCP was capable of enhancing anchorage-independent growth, proliferation, migration, and invasion in vitro, we did not find evidence that RCP alone could induce tumorigenesis in noncancerous cells or promote metastasis of nonmetastatic (MCF7) cells in vivo. Whether RCP alone or in the context of certain other oncogenic signals can drive transformation and/or metastasis warrants further investigation. However, that the growth and metastatic properties of the tumor xenografts were dependent on the endogenous expression of RCP suggests an "oncogene addiction–like" scenario, whereby RCP may play a vital role in the maintenance and potentiation of the malignant and metastatic phenotype.

While the physiological role of RCP is not well understood, evidence from yeast 2-hybrid screens indicates that RCP interacts with RAB25 and RAB11 (20, 21). RCP is thought to interact primarily with RAB11 to regulate protein sorting in tubular endosomes (22). The RAB11-RCP complex has been shown to channel transferrin receptor away from lysosomes (the degradation pathway) to recycling endosomes (the recycling pathway), thereby promoting a relative increase in the steady-state levels of membrane-bound receptors (22). Interestingly, the tumorigenic properties of RAB25 have been linked to a role in recycling endosomes, whereby RAB25 has been observed to mediate the targeted localization of recycling endosomes positive for $\alpha_5\beta_1$ integrin to the plasma surface of pseudopodial tips in a manner that promotes tumor cell invasion (42). Therefore, it is plausible that the oncogenic effects of RCP may be mediated in part by interactions with RAB11 and/or RAB25 that favor protein recycling over degradation, thus enhancing the life span and functionality (or targeted localization) of key membrane proteins such as integrins and growth factor receptors that transmit oncogenic signals. Indeed, during the writing of this manuscript, Caswell and colleagues reported the first detailed mechanism by which RCP could enhance tumor cell migration (43). The authors showed that in the context of inhibition of $\alpha_v\beta_3$ integrin, RCP could form a physical complex with $\alpha_5\beta_1$ integrin and EGFR1 and that this complex not only enhanced recycling of EGFR1 but also enhanced EGFR1 autophosphorylation and downstream signaling. The robust correlation we observed among RCP expression, ERK phosphorylation, and H-RAS activation may also reflect this activity, as it may recapitulate this link between RCP receptor–recycling function and growth factor receptor–mediated MAPK activation. Indeed, endocytosis and endosomal transport of membrane proteins through the cytosol are a requirement for efficient MAPK activation by activated growth factor receptors (44, 45).

On the other hand, coimmunoprecipitation experiments provided evidence of a more direct interaction between RCP and H-RAS that may represent a second, more direct avenue by which RCP exerts its oncogenic influence. RCP in complex with RAB11 localizes to early and recycling endosomes. The primary components of the MAPK pathway, including RAS, RAF1, activated MEK, and MAPK, have all been observed in the endocytic compartment upon stimulation by insulin in HIRcB (rat fibroblast) cells (46, 47) and stimulation by EGF in rat liver (48). In a study by Hancock and colleagues, H-RAS was observed to specifically occupy nascent and recycling endosomes and this occupancy was required for H-RAS but not K-RAS signaling through the RAS/RAF/MAPK cascade (49). Thus, it is plausible that through endosomal colocalization and physical interaction, RCP may drive wild-type H-RAS activation.

Intriguingly, RAS mutations are rarely found in primary breast cancers and their cell lines, whereas they are amply present in other epithelial cancers such as those arising from the colon, thyroid, and lung. In these tissues, activating mutations in RAS proteins, BRAF, and other components upstream of MAPK signaling seldom occur simultaneously in the same tumor. This principle of *mutual exclusivity*, whereby alterations that activate a common oncogenic pathway need not cooccur, suggests that the absence of RAS mutations in breast cancer (and low incident of other RAF/MEK/ERK-activating mutations) may be explained in part by the biochemical activation of RAS through RCP overexpression. In this context, RCP could hold utility as both a biomarker and a target for RAS/MAPK-directed therapeutics.

In conclusion, through integrated genomic analysis, we identified RCP as a candidate oncogene at the 8p11–12 amplicon, with expression levels significantly correlated with aggressive breast cancer behavior. Our functional investigations revealed that RCP plays multiple pathophenotypic roles in breast tumorigenesis that coincide with ERK phosphorylation and RAS activation. That this amplicon has also been observed with frequency in other solid tumors, including non–small cell lung carcinomas (50), colorectal cancer (51), and tumors of the urinary bladder (52) and fallopian tube (53), suggests that RCP may represent a ubiquitous path to cancer progression. The broader involvement of RCP in the pathogenesis of human cancers and the mechanisms underlying its oncogenic effects will be the focus of future investigations.

Methods

Microarray data sets for gene discovery. Raw microarray data (from Affymetrix U133A and U133B GeneChips) were retrieved from Gene Expression Omnibus: the Uppsala cohort (Gene Expression Omnibus accession num-

ber GSE3494) (54), the Stockholm cohort (Gene Expression Omnibus accession number GSE1456) (55), the Oxford cohort (Gene Expression Omnibus accession number GSE6532) (56), and the Singapore cohort (Gene Expression Omnibus accession number GSE4922) (5). Raw data were normalized using the MAS5.0 global mean method (54), with probe set signal intensities scaled to a target signal of 500 and natural log transformed. Of note, sample subsets of 49 and 60 samples within the Oxford and Singapore cohorts, respectively, are currently not included in the GEO database, pending institutional permissions. To minimize cohort-dependent batch effects, arrays within each cohort were mean centered prior to merging into a single data set. Clinical characteristics of all patients and tumor samples are summarized in Table 1.

LSVD. Microarray probe sets were mapped to genomic coordinates using the UCSD Genome Browser. AEFs were inferred by the localized coordinated overexpression of genes in a corresponding subset of tumors. First, a gene was defined as overexpressed in a sample if its expression in that sample was more than 2.5 times the adjusted median absolute deviation (aMAD) from its median expression across all samples. Second, localized coordinated overexpression was quantified by the principal eigenvalue obtained by singular value decomposition (SVD) applied on a sliding window of 50 probes. Probes corresponding to the same gene (according to UniGene ID build no. 177) were averaged to represent a single gene measurement. AEFs were identified as contiguous chromosomal regions having local principal eigenvalues above a baseline threshold. AEFs were scored and ranked by the peak principal eigenvalue. Highest scoring AEFs were subjected to a second round of LSVD using a window size of 10 probes to better resolve peak structure (i.e., to distinguish one from multiple subpeaks). Finally, the highest scoring subpeaks were subjected to SVD to derive eigenweights for the individual genes and tumors. Eigenweights reflect the relative contribution of genes and tumors to the magnitude of a PEP. For a given peak, genes with nonzero eigenweights were considered components of the AEF. Tumors with an eigenweight greater than the median plus 2 SDs were labeled as amplicon-containing tumors (TRIAGE, step 4). Further details of the LSVD procedure are provided in Supplemental Methods.

TRIAGE gene-survival analysis. For each gene, tumors were dichotomized into low expression (below mean) or high expression (above mean) groups, and the Cox proportional hazards regression model was fit to the corresponding patient data to compute a hazard ratio based on DMFS. The null hypothesis was that the 2 groups would have the same risk of recurrence, and the likelihood ratio test *P* value was computed as evidence against this hypothesis. In the case of multiple probe sets mapping to the same gene, the results of the probe set with the most significant association was reported. DMFS was defined as the time interval from surgery until the first distant recurrence event or last date of follow-up. All patients with bilateral and contralateral cancers and those with recurrence or disease-specific death more than 10 years after diagnosis were systematically censored for events. The Uppsala cohort was used to generate the survival data in TRIAGE as it was the largest population-based cohort with the longest and most complete patient follow-up.

Microarray data sets for RAB11FIP/RCP characterization. The correlation of RCP to DMFS was validated using a series of 99 breast tumors from tamoxifen-treated patients with mean follow-up of 5.8 years (56). The MAS5.0 processed and normalized data matrix was downloaded from NCBI's Gene Expression Omnibus database (Gene Expression Omnibus number GSE6532) and used in our analysis without further modifications. LSVD analysis was performed on expression profiles of 19 breast cancer cell lines (57) using the MAS5.0 processed and normalized data matrix provided in the Gene Expression Omnibus entry GSE3156 without further modification. For the correlative analysis of RCP expression and breast cancer progression, a microarray data set comprising normal breast, DCIS, invasive tumor, and nodal metastases was utilized (29). These data, based on a custom Affymetrix array (PDL-Hu03; Gene Expression Omnibus number GSE1477), were only provided as an unlogged, normalized data matrix of average signal intensities, normalized by a γ distribution model. To correct for negative values, each array distribution was shifted toward the positive by adding 1 plus the absolute value of the global minimum intensity. The data were then $\log_2$ transformed and median centered (per array). Only female breast tissue samples were considered for analysis.

Detecting copy number changes. Cell lines were analyzed by array-CGH using the Human Genome CGH Microarray 244A (Agilent Technologies) according to a previously published protocol (58). FISH analysis of cell lines was conducted as previously described (59) using the 8p11–12 BAC probe (overlapping the RCP locus) RP11-933I10.

Selection and cloning of RCP. Three splice variants of RCP were identified in GenBank: variant 1 (GenBank accession number NM_025151), variant 2 (GenBank accession number NM_001002233), and variant 3 (GenBank accession number NM_001002814). Of these, only variants 1 and 3 could be detected consistently in tumor samples and cell lines by RT-PCR (data not shown), and only variant 1 was observed by Western blot with polyclonal RCP antibody (15-288-21574A; GenWay). Thus, the full-length variant 1 of RCP was amplified from normal human blood by RT-PCR (forward primer: 5′-ACCATGTCCCTAATGGTCTCGGCT-3′; reverse primer: 5′-TGCTGATTTACATCTTTCCTCT-3′), sequence verified, and used to investigate RCP function in this study.

Cell lines, constructs, and transient transfection. See Supplemental Methods for additional details. All cell lines were obtained from ATCC and maintained according to ATCC recommendations. RCP-specific RNAi constructs were designed as previously described (60) and manufactured by Ambion (RNAi-RCP1: CGAUAAGCAAGAAGGAGUU) and QIAGEN (RNAi-RCP2: GGAAGGACUUUCCUUUCUU). The specificity of RNAi-RCP1 inhibitory effects (with respect to RCP family members RAB11FIP-2, -3, -4, and -5) was confirmed by real-time PCR in MDA-MB231 and MCF7 cell lines (Supplemental Figure 9).

Generation of stable cell lines by lentiviral infection. See Supplemental Methods for additional details. For the generation of cell lines stably overexpressing shRNA, oligonucleotides encoding the target sequence (forward: 5′-TCGATAAGCAAGAAGGAGTTTTCAAgAgAAACTCCTTCTTGCTTATCGTTTTTTC-3′; and reverse: 5′-TCGAGAAAAAACGATAAGCAAGAAGGAGTTTCTCTTGAAAACTCCTTCTTGCTTATCGA-3′) were annealed and cloned into the LentiLox pLL3.7 vector. For control shRNA, a nontargeting "scramble" sequence was cloned into pLL3.7. (forward: 5′-TGAACGGCATCAAGGTGAACttcaagagaGTTCACCTTGATGCCGTTCTTTTTTC-3′; and reverse: 5′-TCGAGAAAAAAGAACGGCATCAAGGTGAACTCTCTTGAAGTTCACCTTGATGCCGTTCA-3′). For RCP overexpression, full-length RCP was cloned into pENTR3C (Invitrogen) and recombined into pLenti6/V5-DEST (Invitrogen) according to the manufacturer's protocol.

For Western blot and immunohistochemical analysis, cell proliferation and colony formation, invasion and migration assays, immunofluorescence microscopy, and cell-cycle analysis, see Supplemental Methods for details.

Mouse xenograft experiments. All procedures involving the care and sacrifice of animals were approved by the National University of Singapore Institutional Review Board (Singapore) and conducted in accordance with international regulations and Singapore animal holding laws. Female BALB/c-nu/nu (nude) mice and NOD-SCID mice 6 to 8 weeks old were housed under pathogen-free conditions in a temperature-controlled room on a 12-hour light/12-hour dark cycle with food and water ad libitum. For MCF-7 tumor formation experiments, a 1.7-mg 17β-estradiol pellet (90-day release; Innovative Research of America) was implanted (s.c.) in each mouse 1 week prior to tumor cell injection to supplement the estrogen requirements of MCF7

cells. The experimental groups were as follows: (a) BALB/c-nu/nu: MCF7–RNAi RCP (stable RCP knockdown), MCF7–RNAi Ctrl (control), MCF7-RCP (stable overexpression), MCF7-Ctrl (lentivector alone), MB231–RNAi RCP, MB231–RNAi Ctrl, MB231-RCP, MB231-Ctrl, MCF10A-RCP, and MCF10-Ctrl; and (b) NOD-SCID: MB231–RNAi RCP, and MB231–RNAi Ctrl. For each nude mouse experimental group, 8 mice were injected s.c. in both hind flanks with 2.0×10^6 cells suspended in Matrigel. s.c. tumors were measured with a digital caliper weekly. Tumor volume was calculated as $ab^2/2$ in mm^3, where a and b were the longest and the shortest perpendicular diameters of the tumor, respectively. Tumor weights were measured at termination. For each NOD-SCID experimental group, mice were anesthetized with 2,2,2-tribromoethanol, and 1.0×10^6 tumor cells (suspended in 20 ml PBS) were injected into each of the 2 fourth inguinal mammary fat pads (through an incision). The initial study consisted of 9 mice per experimental group, and the size-normalized study consisted of 5 mice per group. The mice were euthanized at 11 weeks, when tumors in the control group reached approximately 1.0 to 1.5 cm in diameter or, for the size-normalized experiments, at 3 weeks (control mice: when tumors reached a size equal to approximately 0.2 grams in weight) or 14 weeks (RNAi RCP mice: to assess metastatic potential over an extended time period). One mouse in the latter group (RNAI RCP) died of dehydration at 10 weeks, and another was sacrificed at 3 weeks for comparison with controls. Tumor, lungs, and other organ tissues were fixed in 10% buffered formalin for 12 hours, washed with PBS, transferred to 70% ethanol, and embedded in paraffin. For assessing tumor RCP levels, tumor sections were incubated with anti-RCP antibody at a 1:500 dilution (using ABC immunohistochemistry reagents and avidin-biotin blocking reagents; Vector Laboratories) prior to counterstaining with hematoxylin. For micrometastasis screening, organ tissues were sectioned at 20 mm intervals. Approximately 50 sections were taken per organ (or 10 sections for the size-normalized experiments), and each section (5-μm thick) was stained with H&E.

Ras-activation assays. Ras activity was determined in stable cell lines overexpressing RCP or shRNA against RCP using a Ras Activation Assay kit (Upstate Biotechnology) according to the manufacturer's protocol.

Coimmunoprecipitation assays. See Supplemental Methods for additional details.

Statistics. Gene expression–survival correlations were computed using Cox proportional-hazards regression and assessed for significance by the likelihood ratio test P value as coded in the R survival package (http://cran.r-project.org/web/packages/survival/index.html). All 2-group statistical comparisons were made using Student's t test (2-tailed). To assess the differential expression of RCP observed between tissue types, t test P values were adjusted for multiple testing using the procedure of Holm (61) to control for FWER. $P < 0.05$ was considered significant.

Acknowledgments

We thank the Singapore Biomedical Research Council and the Singapore Agency for Science, Technology and Research (A*STAR) for funding this work. B. Lim was also supported by grants from the NIH (DK-47636 and AI54973). We also thank Christos Sotiriou (Institut Jules Bordet) and Thomas Lufkin (Genome Institute of Singapore) for helpful discussions and Mik Black (University of Otago) for statistical advice.

Received for publication October 1, 2008, and accepted in revised form May 13, 2009.

Address correspondence to: Lance David Miller, Wake Forest University School of Medicine, Cancer Biology Dept., Medical Center Blvd., Winston-Salem, North Carolina 27157, USA. Phone: (336) 716-6017; Fax: (336) 716-0255; E-mail: ldmiller@wfubmc.edu. Or to: Bing Lim, Genome Institute of Singapore, 60 Biopolis St., #02-01 Genome, Singapore 138672, Singapore. Phone: 65-6478-8156; Fax: 65-6478-9005; E-mail: limb1@gis.a-star.edu.sg.

Jinqiu Zhang's present address is: Stem Cell Disease Models, Institute of Medical Biology, Singapore.

Joshy George's present address is: Peter MacCallum Cancer Centre, East Melbourne, Victoria, Australia.

Nallasivam Palanisamy's present address is: Michigan Center for Translational Pathology, Department of Pathology, University of Michigan, Ann Arbor, Michigan, USA.

Lance David Miller's present address is: Department of Cancer Biology, Wake Forest University School of Medicine, Winston-Salem, North Carolina, USA.

1. Sorlie, T., et al. 2001. Gene expression patterns of breast carcinomas distinguish tumor subclasses with clinical implications. *Proc. Natl. Acad. Sci. U. S. A.* **98**:10869–10874.
2. van 't Veer, L.J., et al. 2002. Gene expression profiling predicts clinical outcome of breast cancer. *Nature.* **415**:530–536.
3. van de Vijver, M.J., et al. 2002. A gene-expression signature as a predictor of survival in breast cancer. *N. Engl. J. Med.* **347**:1999–2009.
4. Sotiriou, C., et al. 2006. Gene expression profiling in breast cancer: understanding the molecular basis of histologic grade to improve prognosis. *J. Natl. Cancer Inst.* **98**:262–272.
5. Ivshina, A.V., et al. 2006. Genetic reclassification of histologic grade delineates new clinical subtypes of breast cancer. *Cancer Res.* **66**:10292–10301.
6. Hicks, J., et al. 2006. Novel patterns of genome rearrangement and their association with survival in breast cancer. *Genome Res.* **16**:1465–1479.
7. Bergamaschi, A., et al. 2006. Distinct patterns of DNA copy number alteration are associated with different clinicopathological features and gene-expression subtypes of breast cancer. *Genes Chromosomes Cancer.* **45**:1033–1040.
8. Jenssen, T.K., Kuo, W.P., Stokke, T., and Hovig, E. 2002. Associations between gene expressions in breast cancer and patient survival. *Hum. Genet.* **111**:411–420.
9. Adler, A.S., et al. 2006. Genetic regulators of large-scale transcriptional signatures in cancer. *Nat. Genet.* **38**:421–430.
10. Adler, A.S., and Chang, H.Y. 2006. From description to causality: mechanisms of gene expression signatures in cancer. *Cell Cycle.* **5**:1148–1151.
11. Chin, K., et al. 2006. Genomic and transcriptional aberrations linked to breast cancer pathophysiologies. *Cancer Cell.* **10**:529–541.
12. Miller, L.D., and Liu, E.T. 2007. Expression genomics in breast cancer research: microarrays at the crossroads of biology and medicine. *Breast Cancer Res.* **9**:206.
13. Stransky, N., et al. 2006. Regional copy number-independent deregulation of transcription in cancer. *Nat. Genet.* **38**:1386–1396.
14. Reyal, F., et al. 2005. Visualizing chromosomes as transcriptome correlation maps: evidence of chromosomal domains containing co-expressed genes--a study of 130 invasive ductal breast carcinomas. *Cancer Res.* **65**:1376–1383.
15. Pollack, J.R., et al. 2002. Microarray analysis reveals a major direct role of DNA copy number alteration in the transcriptional program of human breast tumors. *Proc. Natl. Acad. Sci. U. S. A.* **99**:12963–12968.
16. Ray, M.E., et al. 2004. Genomic and expression analysis of the 8p11-12 amplicon in human breast cancer cell lines. *Cancer Res.* **64**:40–47.
17. Garcia, M.J., et al. 2005. A 1 Mb minimal amplicon at 8p11-12 in breast cancer identifies new candidate oncogenes. *Oncogene.* **24**:5235–5245.
18. Gelsi-Boyer, V., et al. 2005. Comprehensive profiling of 8p11-12 amplification in breast cancer. *Mol. Cancer Res.* **3**:655–667.
19. Letessier, A., et al. 2006. Frequency, prognostic impact, and subtype association of 8p12, 8q24, 11q13, 12p13, 17q12, and 20q13 amplifications in breast cancers. *BMC Cancer.* **6**:245.
20. Hales, C.M., et al. 2001. Identification and characterization of a family of Rab11-interacting proteins. *J. Biol. Chem.* **276**:39067–39075.
21. Lindsay, A.J., et al. 2002. Rab coupling protein (RCP), a novel Rab4 and Rab11 effector protein. *J. Biol. Chem.* **277**:12190–12199.
22. Peden, A.A., et al. 2004. The RCP-Rab11 complex regulates endocytic protein sorting. *Mol. Biol. Cell.* **15**:3530–3541.
23. Gebhardt, C., et al. 2005. c-Fos-dependent induction of the small ras-related GTPase Rab11a in skin

carcinogenesis. *Am. J. Pathol.* **167**:243–253.
24. Goldenring, J.R., Ray, G.S., and Lee, J.R. 1999. Rab11 in dysplasia of Barrett's epithelia. *Yale J. Biol. Med.* **72**:113–120.
25. Yoon, S.O., Shin, S., and Mercurio, A.M. 2005. Hypoxia stimulates carcinoma invasion by stabilizing microtubules and promoting the Rab11 trafficking of the alpha6beta4 integrin. *Cancer Res.* **65**:2761–2769.
26. Cheng, K.W., et al. 2004. The RAB25 small GTPase determines aggressiveness of ovarian and breast cancers. *Nat. Med.* **10**:1251–1256.
27. Cheng, K.W., Lu, Y., and Mills, G.B. 2005. Assay of Rab25 function in ovarian and breast cancers. *Methods Enzymol.* **403**:202–215.
28. Calza, S., et al. 2006. Intrinsic molecular signature of breast cancer in a population-based cohort of 412 patients. *Breast Cancer Res.* **8**:R34.
29. Radvanyi, L., et al. 2005. The gene associated with trichorhinophalangeal syndrome in humans is overexpressed in breast cancer. *Proc. Natl. Acad. Sci. U. S. A.* **102**:11005–11010.
30. Perou, C.M., et al. 2000. Molecular portraits of human breast tumours. *Nature.* **406**:747–752.
31. Adnane, J., et al. 1991. BEK and FLG, two receptors to members of the FGF family, are amplified in subsets of human breast cancers. *Oncogene.* **6**:659–663.
32. Theillet, C., et al. 1993. FGFRI and PLAT genes and DNA amplification at 8p12 in breast and ovarian cancers. *Genes Chromosomes Cancer.* **7**:219–226.
33. Cuny, M., et al. 2000. Relating genotype and phenotype in breast cancer: an analysis of the prognostic significance of amplification at eight different genes or loci and of p53 mutations. *Cancer Res.* **60**:1077–1083.
34. Streicher, K.L., Yang, Z.Q., Draghici, S., and Ethier, S.P. 2007. Transforming function of the LSM1 oncogene in human breast cancers with the 8p11-12 amplicon. *Oncogene.* **26**:2104–2114.
35. Yang, Z.Q., Streicher, K.L., Ray, M.E., Abrams, J., and Ethier, S.P. 2006. Multiple interacting oncogenes on the 8p11-p12 amplicon in human breast cancer. *Cancer Res.* **66**:11632–11643.
36. Jaffe, A.B., and Hall, A. 2005. Rho GTPases: biochemistry and biology. *Annu. Rev. Cell Dev. Biol.* **21**:247–269.
37. Li, X., and Lim, B. 2003. RhoGTPases and their role in cancer. *Oncol. Res.* **13**:323–331.
38. Jones, M.C., Caswell, P.T., and Norman, J.C. 2006. Endocytic recycling pathways: emerging regulators of cell migration. *Curr. Opin. Cell Biol.* **18**:549–557.
39. Damiani, M.T., et al. 2004. Rab coupling protein associates with phagosomes and regulates recycling from the phagosomal compartment. *Traffic.* **5**:785–797.
40. Powelka, A.M., et al. 2004. Stimulation-dependent recycling of integrin beta1 regulated by ARF6 and Rab11. *Traffic.* **5**:20–36.
41. Neve, R.M., et al. 2006. A collection of breast cancer cell lines for the study of functionally distinct cancer subtypes. *Cancer Cell.* **10**:515–527.
42. Caswell, P.T., et al. 2007. Rab25 associates with alpha5beta1 integrin to promote invasive migration in 3D microenvironments. *Dev. Cell.* **13**:496–510.
43. Caswell, P.T., et al. 2008. Rab-coupling protein coordinates recycling of alpha5beta1 integrin and EGFR1 to promote cell migration in 3D microenvironments. *J. Cell Biol.* **183**:143–155.
44. Vieira, A.V., Lamaze, C., and Schmid, S.L. 1996. Control of EGF receptor signaling by clathrin-mediated endocytosis. *Science.* **274**:2086–2089.
45. Ceresa, B.P., and Schmid, S.L. 2000. Regulation of signal transduction by endocytosis. *Curr. Opin. Cell Biol.* **12**:204–210.
46. Rizzo, M.A., Shome, K., Watkins, S.C., and Romero, G. 2000. The recruitment of Raf-1 to membranes is mediated by direct interaction with phosphatidic acid and is independent of association with Ras. *J. Biol. Chem.* **275**:23911–23918.
47. Rizzo, M.A., Kraft, C.A., Watkins, S.C., Levitan, E.S., and Romero, G. 2001. Agonist-dependent traffic of raft-associated Ras and Raf-1 is required for activation of the mitogen-activated protein kinase cascade. *J. Biol. Chem.* **276**:34928–34933.
48. Pol, A., Calvo, M., and Enrich, C. 1998. Isolated endosomes from quiescent rat liver contain the signal transduction machinery. Differential distribution of activated Raf-1 and Mek in the endocytic compartment. *FEBS Lett.* **441**:34–38.
49. Roy, S., Wyse, B., and Hancock, J.F. 2002. H-Ras signaling and K-Ras signaling are differentially dependent on endocytosis. *Mol. Cell. Biol.* **22**:5128–5140.
50. Balsara, B.R., et al. 1997. Comparative genomic hybridization analysis detects frequent, often high-level, overrepresentation of DNA sequences at 3q, 5p, 7p, and 8q in human non-small cell lung carcinomas. *Cancer Res.* **57**:2116–2120.
51. Nakao, K., et al. 2004. High-resolution analysis of DNA copy number alterations in colorectal cancer by array-based comparative genomic hybridization. *Carcinogenesis.* **25**:1345–1357.
52. Simon, R., et al. 2001. High-throughput tissue microarray analysis of 3p25 (RAF1) and 8p12 (FGFR1) copy number alterations in urinary bladder cancer. *Cancer Res.* **61**:4514–4519.
53. Snijders, A.M., et al. 2003. Genome-wide-array-based comparative genomic hybridization reveals genetic homogeneity and frequent copy number increases encompassing CCNE1 in fallopian tube carcinoma. *Oncogene.* **22**:4281–4286.
54. Miller, L.D., et al. 2005. An expression signature for p53 status in human breast cancer predicts mutation status, transcriptional effects, and patient survival. *Proc. Natl. Acad. Sci. U. S. A.* **102**:13550–13555.
55. Pawitan, Y., et al. 2005. Gene expression profiling spares early breast cancer patients from adjuvant therapy: derived and validated in two population-based cohorts. *Breast Cancer Res.* **7**:R953–R964.
56. Loi, S., et al. 2007. Definition of clinically distinct molecular subtypes in estrogen receptor-positive breast carcinomas through genomic grade. *J. Clin. Oncol.* **25**:1239–1246.
57. Bild, A.H., et al. 2006. Oncogenic pathway signatures in human cancers as a guide to targeted therapies. *Nature.* **439**:353–357.
58. Poonepalli, A., et al. 2008. Telomere-mediated genomic instability and the clinico-pathological parameters in breast cancer. *Genes Chromosomes Cancer.* **47**:1098–1109.
59. Ruan, Y., et al. 2007. Fusion transcripts and transcribed retrotransposed loci discovered through comprehensive transcriptome analysis using Paired-End diTags (PETs). *Genome Res.* **17**:828–838.
60. Reynolds, A., et al. 2004. Rational siRNA design for RNA interference. *Nat. Biotechnol.* **22**:326–330.
61. Holm, S. 1970. A simple sequentially rejective multiple test procedure. *Scandinavian Journal of Statistics.* **6**:65–70.